Interfacial Velocity-Dependent Plasmon Damping in Colloidal Metallic Nanoparticles

R. Zadoyan

Technology and Applications Center, Newport Corporation, 1791 Deere Avenue, Irvine, California 926006

H. Ye. Seferyan, A. W. Wark, R. M. Corn, and V. A. Apkarian*

Department of Chemistry, University of California, Irvine, California 92697

Received: February 26, 2007; In Final Form: May 9, 2007

Modulation of the surface plasmon resonance of colloidal silver nanoparticles driven by particle shape oscillations is interrogated via transient-scattering measurements using white light as the probe. The two-dimensional (λ, t) image of the spectrally resolved scattering shows $\pi/2$ phase shift between the modulation of center $\Omega(t)$ and width $\Gamma(t)$ of the resonance − while Ω is modulated by the strain amplitude, the plasmon-damping rate Γ is modulated by the strain rate. We ascribe the effect to scattering from the electrophoretic potential generated by the motion of the interfacial double layer of the colloidal particles.

Introduction

Plasmon resonances of metallic nanoparticles have been of historical interest, first quantified by Mie for the case of spherical particles.[1] Presently, they are the subject of great interest due to the multitude of applications enabled by locally enhanced electric fields and nonlinear optical phenomena mediated by them.[2,3] The optical properties of nanoparticles, summarized by their extinction spectra, depend on size, shape, dielectric medium, and interfacial structure.[4] Beyond the Mie theory, numerical solutions of Maxwell's equations are used to compute spectra of arbitrary structures.[5] The success of such treatments has been validated in light-scattering measurements on single particles that are simultaneously characterized through microscopy.[6−8] Time-resolved measurements, although carried out on ensembles of particles, provide the dynamical connection between structure and optical response, and as such can lead to a more detailed characterization of properties. Ultrafast pump−probe measurements have been used to monitor the damping of surface plasmons in real-time.[9−11] It is well established that the damping rate of the collective electron motion, Γ, (the sum of dephasing and dissipation) determines the width of the spectral response. Accordingly, the extinction spectra, $\sigma(\omega,t)$, can be approximated as Lorentzian, defined by the two moments: line-center, Ω, and line-width, Γ. It is also well established that the dissipation of plasmons through electron−phonon scattering is completed on the time scale of 10^{-12} s. As such, optical excitation of nanoparticles with subpicosecond pulses leads to a sudden jump in lattice temperature and drives the particles into shape oscillations. This in turn leads to the modulation of plasmon resonances on time scales of 1 ps $< t <$ 1 ns, as observed in transient-scattering spectroscopy.[12] The period of modulation and its damping rate can be gainfully employed to extract mechanical and thermal properties of particles, as demonstrated on gold spheres and nanorods,[13] silver spheres,[14] ellipsoids,[15] prisms,[16,17] and triangular nanoplates.[18] The only assumption necessary for such analyses is for the resonance, Ω, to be modulated by the mechanical vibrations of the particle. The microscopic connection is suggested by noting that because the free plasmon frequency, $\omega_p = (ne^2/\epsilon_0 m_e)^{1/2}$, is determined by the electron density, $n = N/V$, then volume oscillations should modulate the resonance frequency, $\delta\Omega/\Omega = \delta\omega_p/\omega_p = -\delta V/2V$. This is clearly an oversimplification of the dynamics; it ignores the dielectric response of the medium and does not leave room for the interpretation of modulations in Γ, which is observed in most reported measurements. Spectrally resolved transient scattering provides two-dimensional (2D) images of $\sigma(\omega,t)$, mapping the dynamical correlation between Ω and Γ. Our measurements on colloidal silver nanorods show a $\pi/2$ phase shift between line-center and line-width, indicating that the spectral response contains a component that tracks the particle strain rate. We ascribe the effect to the dynamical response of the interfacial double-layer present in all colloidal preparations and estimate the magnitude of the effect to be in accord with the observation. Some of the implications of this novel finding are addressed.

Sample Preparation

Colloidal silver nanoparticles were prepared by citrate reduction of silver salt using a standard chemical recipe.[19,20] Briefly, 200 mL of Millipore-filtered water was heated until approximately 40°C at which 36 mg of $AgNO_3$ was added. Heating and vigorous stirring was continued until the solution approached boiling point and 4 mL of 1% w/v trisodium citrate was added. After further stirring for 1 h, the solution was cooled to room temperature. The preparation was stored at 4°C and remained stable with no significant change in absorption spectrum over a period of 6 months. The UV−vis absorption spectrum of the sample is shown in Figure 1a. The spectrum shows the plasmon resonance near 420 nm, characteristic of the nominal particle sizes and dispersion in sizes. The transmission electron microscope (TEM) image in Figure 1b shows that the sample contains a wide distribution of particle sizes and shapes. The experiments we report are highly selective. Only the subset of nanorods with large aspect ratio is interrogated. This is accomplished by taking advantage of the photolability of silver particles. Extensive irradiation at 800 nm generates a hole in the inhomogeneous spectral profile with concomitant

* To whom correspondence should be addressed. E-mail: aapkaria@uci.edu.

10.1021/jp0715979 CCC: $37.00
Published on Web 06/23/2007

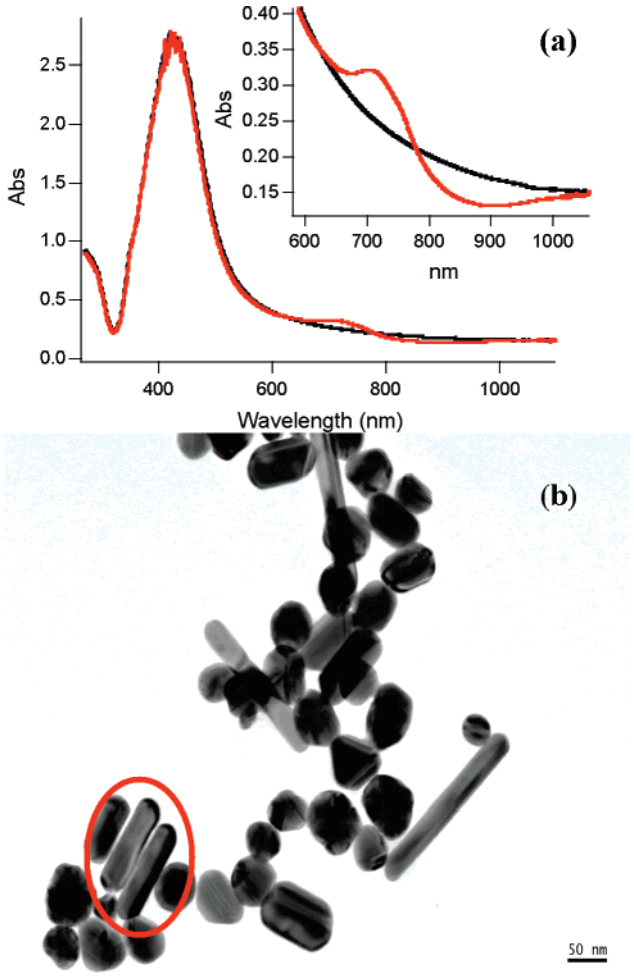

Figure 1. (a) Absorbance of colloidal silver nanoparticles dispersed in water. Solid black line, initial spectrum before exposure to 800 nm radiation; red line, after exposure to radiation for 60 min. The inset magnifies the observed change in the spectrum. (b) TEM image of the silver nanoparticles used in the experiment shows a broad dispersion in size and shape. The experiment selects rods with dimensions that are consistent with the two nanorods seen in the lower left corner of the image.

growth of a new absorption near 705 nm, as illustrated in the inset to Figure 1a. The time-resolved-scattering measurements yield the modulation of this relatively sharp resonance, without any contributions from the inhomogeneous background. The analysis of the plasmon modulation period and cooling rate establishes that nanorods of a narrow distribution is interrogated, as we expand below.

Experimental Methods

The transient absorption measurements are carried out using a commercial spectrometer (Helios, Newport). On the basis of an amplified Ti:Sapphire femtosecond laser operating at 5 kHz (Tsunami, Spitfire Pro 40F, Spectra-Physics), the system relies on white light generated in a sapphire substrate as the probe. The fundamental of the Ti:Sapphire laser at 800 nm is used as the pump source. The transmitted white light is dispersed in a 1/8 m fiber-coupled spectrograph, and the spectrum between 400 and 800 nm is recorded with a CCD array. The pump beam is chopped at 2.5 kHz, and the pulse-to-pulse differential absorbance $\Delta A = -\log_{10}(T_{on}/T_{off})$ where T_{on} and T_{off} are the transmitted intensities with pump-on and pump-off is recorded as a function of delay between pump and white-light probe.

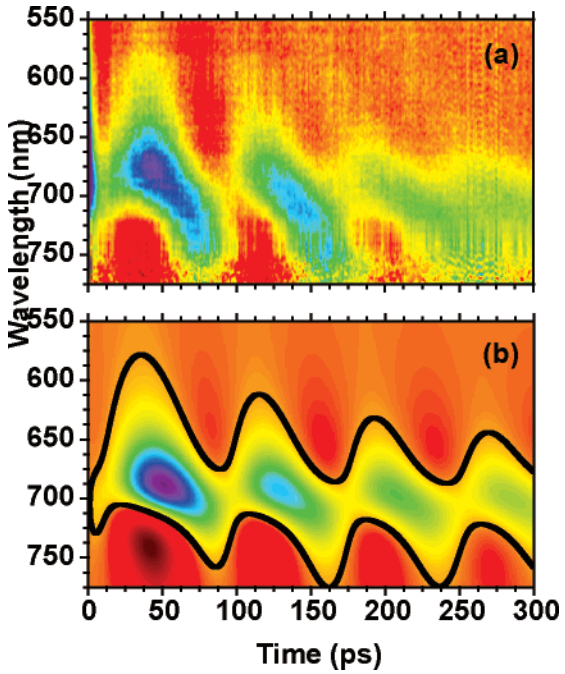

Figure 2. (a) Image plot of time- and frequency-resolved transient absorbance upon excitation at 800 nm. (b) Global fit according to the model introduced in the text.

Although the white light is chirped, the spectrally resolved detection allows transient absorption detection at a given wavelength with a resolution of 40 fs and a sensitivity of $\Delta A = 10^{-4}$.

Results and Analysis

The image plot of the spectrally resolved transient absorbance upon pumping at 800 nm is shown in Figure 2. Two time slices taken at wavelengths where the oscillations are antiphase are shown in Figure 3. The slices are bipolar, they oscillate about zero, as such, they interweave. For a weakly scattering sample, the signal ΔA can be well thought of as the difference of the extinction spectra before and after the excitation (to within a small constant c)

$$\Delta A(\omega,t) = c\left[\frac{\Gamma_0}{(\omega-\Omega_0)^2-\Gamma_0^2/4} - \frac{\Gamma(t)}{(\omega-\Omega(t))^2-\Gamma(t)^2/4}\right] \quad (1)$$

where both $\Omega(t)$ and $\Gamma(t)$ are oscillatory functions that damp out in time. The $\Delta A = 0$ contour line, which is included in the image of Figure 2, shows the cross modulation between the two functions. Similar to a Lissajou figure, the contour uniquely identifies that the two functions have the same period of oscillation but are phase shifted by $\pi/2$. Measurements as a function of pump intensity indicate that the observed response is strictly linear; the signal is the result of time-dependent linear extinction, which is the sum of absorption and scattering. The identical signal is obtained when the pump polarization is rotated by 90° relative to the probe, except for approximately a 3-fold drop in overall intensity. Evidently, the excitation is parallel to the polarization of the pump field.

The signal can be well reproduced by treating the motion of the metal particle as a forced, damped oscillator

$$\ddot{x} + \frac{2}{\tau_d}\dot{x} + \left(\frac{2\pi}{\tau}\right)^2(x - x_0 - \alpha\Delta T(t)) = 0 \quad (2)$$

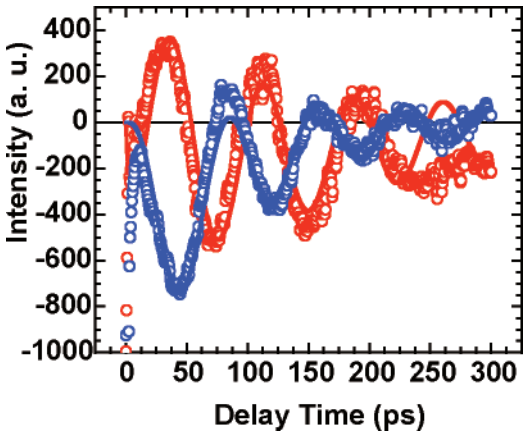

Figure 3. Two time slices taken at wavelengths where the oscillations are antiphase with corresponding fits according to the described model. Red circles, time-resolved transient absorbance at 725 nm; blue circles, time-resolved transient absorbance at 650 nm; solid lines are the corresponding fits.

in which τ is the harmonic period of the oscillator, τ_d is the time constant for mechanical damping, and the forcing function represents the thermal strain

$$\Delta T(t) = \Delta T_0[\exp(-t/\tau_c) - \exp(-t/\tau_h)] \qquad (3)$$

where α is the thermal expansion coefficient, ΔT_0 determines the temperature jump of the lattice, and τ_h and τ_c are the time constants for lattice heating and cooling, respectively. The time profile in eq 3 ignores the evolution of the electron temperature at early time; it applies for the long-time evolution of the lattice temperature, which is the focus of our report. The trajectory of the oscillator serves as the ancillary function to fit the 2D data with

$$\Omega(t) = \Omega_0 + c_1(x(t) - x_0) \qquad (4)$$

and

$$\Gamma(t) = \Gamma_0 + c_2\dot{x}(t) + c_3\Delta T(t) \qquad (5)$$

The last term in eq 5 represents the thermal contribution to line broadening. Although essential, the functional form of this term is not uniquely determined by the data (see below). The essential ingredients of the simulation are that the line-center is modulated by the strain $\epsilon = \Delta x/x_0 = x(t)/x_0 - 1$, while the line-width is modulated by the strain rate, $\dot{\epsilon} = \dot{x}(t)/x_0$. The simulated image captures all features of the experiment, as evident in the comparison in Figure 2, panels a and b. The comparison in the time slices of Figure 3 is also quite satisfactory, except in the last period of motion where the modulation depth in the simulation is deeper than in the experiment. This may be attributed to the fact that inhomogeneous dephasing is entirely neglected in the analysis. Indeed, at a given spectral slice dephasing due to the polydispersity of the sample is minimal, as evidenced by the fact that the signal remains oscillatory as it damps out (the signature of inhomogeneous dephasing is the development of a non-oscillatory exponential tail). However, there is a measurable variation in the period of oscillation with wavelength.

The parameters of the fit provide valuable insights. The time constants in eqs 2 and 3 are well determined. The period of motion is 76 ps and shows a chirp of ~1 ps per period, which is included in the treatment as a refinement. The period also shows spectral dispersion, which ranges from 75 to 80 ps over

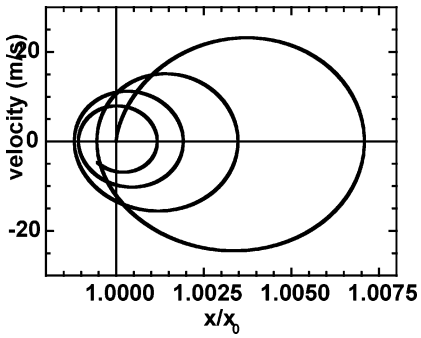

Figure 4. Phase portrait of the oscillator.

the 100 nm span between 625 and 725 nm. The interweaving of signals taken on either side of the line-center (Figure 3) necessarily implies that the damping time is long compared to the cooling time. This generates the phase portrait of the oscillator shown in Figure 4, in which the oscillator contracts beyond its original length, x_0; as it cools, it oscillates about x_0 generating the zero crossings of the signal amplitude seen in Figure 3. The fit parameters are $\tau_d = 200$ ps and $\tau_c = 65$ ps. That the cooling time is shorter than the period of motion implies that two different length scales determine the thermal and mechanical properties; the observed particles are not spherical, but rather rodlike. The dimensions can then be established by noting that for a rod, the lowest-vibrational mode is the longitudinal extension with period $\tau = 2L(\rho/E)^{1/2}$ given by the density, ρ , and Young's modulus, E. Using parameters of bulk silver, the length of the rod can be estimated as $L = 97 \pm 6$ nm. The 6% dispersion in length is directly obtained from the observed spectral dispersion in period. Through the use of the commonly employed model for cooling,[21] the cooling time for a cylinder with spherical caps can be derived from

$$\tau_c = \left\{\frac{4R^2 + 3R(d-2R)}{12R + 6(d-2R)}\right\}^2 \frac{\rho_{Ag}{}^2 C_{Ag}{}^2}{\rho_s C_s \Lambda_s} \qquad (6)$$

where ρ and C are density and heat capacity of silver (Ag) or solvent (s), and Λ_s is the thermal conductivity of the solvent (water in the present). Through the use of the known values of bulk silver and water, $\tau_c = 65$ ps yields a rod radius $R = 10$ nm. The observed particles are essentially monodisperse nanorods of aspect ratio ~1/5. Although the TEM shows a very large distribution in sizes and shapes, the experiment is highly selective. The nanorod dimensions extracted from the dynamical analysis are close to the prominent subensemble of rods circled in the TEM image in Figure 1b, which shows $L = 110$ nm and $R = 15$ nm.

The above thermal and mechanical analysis does not require a microscopic model regarding the connection between the optical response and the underlying dynamics. This connection is coded in the parametrization of $\Omega(t)$ and $\Gamma(t)$ in eqs 4 and 5 with extracted functions graphed in Figure 5. The center of the plasmon band $\lambda(t)$ oscillates around its original position $\lambda_0 =$ 705 nm with maximum amplitude of $\Delta\lambda \approx 2.25$ nm. The plasmon bandwidth $\Gamma(t)$ extracted from the analysis broadens from its original value $\Gamma_0 = 235$ meV $= 90$ nm and oscillates with the same period as the center of the plasmon band but with $\pi/2$ phase shift and with amplitude of $\Delta\Gamma \approx 6.2$ meV $=$ 2.3 nm. The plasmon frequency depends on the strain amplitude of the nanorod, which would yield itself to the interpretation that it is determined by the electron density modulated by the volume oscillations. For extensional modes that nearly preserve the cross-sectional area, this would suggest $\delta\lambda/\lambda = \delta L/2L \approx$

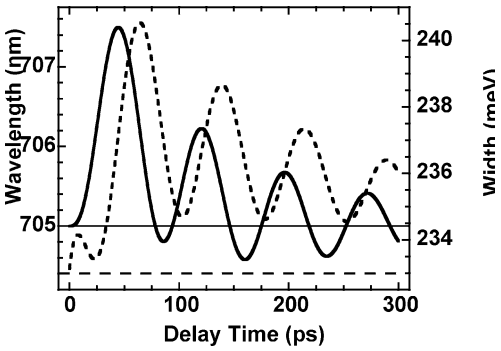

Figure 5. Solid line: peak position (in wavelength units) of the plasmon band, $\Omega(t)$, vs time, determined from analysis of the transient absorbance data in Figure 2a. Dashed line: modulation of the width of the plasmon band $\Gamma(t)$. Although both oscillate with the same frequency of the oscillator, $\pi/2$ phase shift is clearly seen. Horizontal solid and dashed lines mark the original values of the peak position and the width of surface plasmon resonance.

0.3% . For nanorods of length $L \sim 100$ nm, the implied total extension is $\delta L \sim 0.6$ nm. The rate of extension is $\dot{x} \sim 0.01$ nm/ps $= 10$ m/s. Also, for linear thermal strain, $\delta L/L = \alpha \delta T$, a temperature rise of 220°K is implied ($\Delta T_0 = 400$°K in eq 3).

The modulation of the line-width does not lend itself to such a simple model. The recognized contributions to the damping rate of plasmons in nanoparticles are the bulk,[22] surface,[23] radiative,[2] and interfacial[22,24] terms

$$\Gamma = \gamma_b + \gamma_s + \gamma_r + \gamma = \gamma_b + \frac{A\upsilon_F}{L_{eff}} + \frac{h\kappa V}{\pi} + \gamma_i \quad (7)$$

In the size range where the dimensions of the particle become comparable to the electron-scattering length in the bulk, the surface term dominates. The surface contribution can be cast in classical terms,[23] $\gamma_s = A\upsilon_F/L_{eff}$, where L_{eff} is the effective-scattering length that can be defined for arbitrary shapes and sizes[25] and the proportionality constant is determined experimentally as $A \sim 0.3$. The radiative-damping contribution becomes important for the larger particles, because its contribution grows with volume, V. The interfacial term is less specific. It is used to describe scattering from the molecular structure at the metal−medium interface, especially where chemical bonding occurs. This contribution is clearly identified in the small size range of a few nm.[26] None of these sources contains a velocity-dependent term. Moreover, the disparity between the velocity of the body motion, $\dot{x} = 10$ m/s, and the Fermi velocity of the electron of $\upsilon_F = 10^6$ m/s precludes a mechanical contribution of scattering from a moving surface to be of significance to effect γ. Similarly, during the lifetime of the plasmon of 10^{-13} s the volume can be regarded as stationary, and therefore velocity-dependent contributions to radiative damping may be discounted. Shape oscillations of the particles can modulate the line-width through both the surface and radiative terms, through oscillations of υ_F,[27] L_{eff},[28] and V, but such shape-dependent modulation can only be in-phase or counter-phase to strain oscillations. The known channels of plasmon damping do not admit a velocity-dependent term.

The full dynamical description of an impulsively driven nanoparticle with electron density in contact with a fluid is rather rich. The prototypical system of a Rydberg or excess electron in a simple liquid, such as helium, illustrates some of the considerations.[29,30] Under the most gentle of conditions, the impulsively driven compressible electron gas elicits viscoelastic response from the fluid, leading to interfacial thinning, density fluctuations in the near field, and radiation of sound in the far field. With a temperature jump of ~200° K and 0.6 nm extension along the poles where the plasmon extends into the liquid, a significantly larger perturbation of the medium and its dielectric response is to be expected. In our analysis, we find the presence of surface charge to play the key role. Colloidal preparations invariably require surface-bound charge (citrate ions in the present) to prevent aggregation or flocculation. The surface-bound charge layer (Nernst layer) sustains an interfacial electric field $E_{int} = 4\pi\sigma/\epsilon_m$ (σ is the charge per unit area and ϵ_m is the dielectric of the electrolyte), which serves as a scattering force $-eE$, on the metal electrons. The sudden heating of the solvent shell will also lead to a drop in ϵ_m[31] and therefore a rise in E_{int}. This provides for a T-dependent mechanism for line broadening (last term in eq 5). Now consider the effect of shape oscillations of the colloidal particle. The surface-bound charge layer moves with the extensional velocity $\dot{x}$, while the diffuse double-layer response is limited by ionic mobility. The motion of a charged interface in an electrolyte generates the electrophoretic field E_{ep}[32]

$$E_{ep} = \frac{4\pi\eta}{\epsilon_m\zeta}\dot{x} \quad (8)$$

in which ζ is the so-called zeta potential determined by the thickness of the Nernst layer and η is the viscosity of the fluid. The time-dependent damping of the plasmon can then be obtained by considering the scattering rate of Fermi electrons (with momentum $\hbar k_F$) on the combined fields

$$\gamma(t) = \frac{1}{k_F}\frac{dk}{dt} = \frac{1}{\hbar k_F}e(E_{ep} + E_{int}) = \left(\frac{V}{3\pi^2 N}\right)^{1/3}\frac{e(E_{ep} + E_{int})}{\hbar} = \left(\frac{V}{3\pi^2 N}\right)^{1/3}\frac{4\pi e}{\hbar}\left(\frac{\eta}{\epsilon_m\zeta}\dot{x}(t) + \frac{\sigma}{\epsilon_m(t)}\right) \quad (9)$$

which can be recast in the form of the phenomenological function eq 5 used in the data analysis with the assumption $\epsilon_m(t) \propto 1/\Delta T_s(t) + \gamma_0'$ (note, the product $\epsilon_m\zeta$ is time independent, and γ_0' is contained in the stationary term in eq 5), where $\Delta T_s(t)$ is the change of temperature in the surrounding liquid, which cools down on a longer time scale than the nanorod. The magnitude of the velocity-dependent modulation of the line width can be estimated. At an interfacial velocity $\dot{x} \sim 10$ m/s, an electrophoretic field of $E_{ep} = 10^8$ V/m is to be expected for a typical value of $\zeta = 30$ mV in water.[32] Through the use of the electron density of bulk silver in eq 9, a scattering rate of $\gamma_{ep} = 1.2 \times 10^{13}$ s^{-1} is obtained, that is, a contribution to line-width of ~10 meV, which is in quantitative agreement with the experiment (see Figure 5).

While the recognition of plasmon-damping rate determined by the strain rate of the nanoparticle is novel, the phenomenon is evident in prior time- and spectrally resolved light-scattering measurements carried out on colloidal metallic nanoparticles. A $\pi/2$ phase shift between $\Omega(t)$ and $\Gamma(t)$ is reported in very similar experiments performed on triangle-shaped silver nanoplates with the suggestion that this arises from a second vibrational mode of the particle launched with a coincidental time delay.[18] Similarly, the reported data on gold nanospheres[33] and gold nanorods[11] also show a $\pi/2$ phase shift in the modulation of line width; however, neither the origin of this modulation nor the phase shift has been addressed. The relative magnitudes of the observed modulation vary, depending on the nature of the metal, the preparation, and the medium. Consistent

with the literature data, we find that the line-width oscillations are smaller in gold than in silver. In effect, the phenomenon is general and measurement artifacts, such as inhomogeneous dynamics of distributions, can be discounted. Our interpretation of the effect in terms of the electric double-layer also finds support in a recent spectroelectrochemical measurement in which the plasmon resonance of 2D silver arrays was shown to be modulated by an applied external field.[34]

Concluding Remarks

We demonstrate that the plasmon line-width of colloidal silver nanorods is modulated by the strain rate of the particle. We ascribe the effect to electron damping by the electrophoretic potential arising from the motion of a charged interface in a dielectric and quantitatively reproduce the observed magnitude of line-breathing. The effect is recognized as broadly applicable to colloidal particles, which necessarily carry an electric double layer. In effect, the nanoparticles act as acousto−optical transducers; the plasmon resonance responds to the disturbance of the electric double layer and converts the acoustic motion into an optical signal. The mechanism is analogous to the operation of an electret microphone, where the distortion of surface capacitance generates an electric signal. In principle, it should be possible to use the particles to detect electrolytic motion at the interface through the streaming potential and to use them as nanovelocimeters.

It is also remarkable that the experiment selects a nearly monodisperse subensemble of nanorods for interrogation, although TEM shows a very wide distribution of shapes and sizes. The selectivity is achieved by two considerations. Irradiation in the far-red tail of the extinction curve with a relatively narrow bandwidth laser ensures that a small subensemble is excited; long nanorods that can be seen in the TEM of Figure 1b, which preferentially absorb at 800 nm. It is not surprising that resonant irradiation at intensities of μJ/mm^2 leads to destruction of such rods, as verified by the formation of a spectral hole in unstirred samples (Figure 1a). What is surprising is that the resulting daughter particles are quite monodisperse; the rods must pinch-off at a characteristic length, which we surmise to be determined by the coherence length of the plasmon. Once a new spectral feature (antihole) is generated on a broad background, the transient-scattering measurement only shows the modulation of the narrow feature. The shape of the observed particles as nanorods is identified by the different length scales involved in thermal cooling and mechanical vibration; cooling is determined by the short dimension, the radius of the particle, while the body vibrations are determined by the extensional mode, namely, the length of the rod. That the length extracted from the vibrational period underestimates the TEM-measured length, as has been noted previously,[7] we ascribe this to the neglect of fluid dragged by the motion; the effective mass of an oscillator in a liquid is augmented by the mass of the displaced liquid.

The present analysis was aimed mainly at identifying the dominant effects in the observables. A more detailed analysis, perhaps through simulation, would be quite valuable in providing a deeper understanding of the interfacial dynamics and the response of collective electrons to time-dependent density fluctuations of the plasmon and the surrounding electrolytic fluid.

Acknowledgment. This research was funded through the NSF Chemical Bonding Center (CHE-0533162). A.W.W. and R.M.C. acknowledge funding support from the National Institute of Health (2RO1 GM059622-04) and the National Science Foundation (CHE-0551935).

References and Notes

(1) Mie, G. *Ann. Phys.* **1908**, *25*, 377.
(2) Wokaun, A.; Gordon, J. P.; Liao, P. F. *Phys. Rev. Lett.* **1982,** *48*, 957.
(3) Kneipp, K.; Wang, Y.; Kneipp, H.; Perelman, L. T.; Itzkan, I.; Dasari, R.; Feld, M. S. *Phys. Rev. Lett*. **1997,** *78*, 1667.
(4) Link, S.; El-Sayed, M. A. *Int. Rev. Phys. Chem*. **2000,** *19*, 409.
(5) Kelly, K. L.; Coronado, E.; Zhao, L. L.; Schatz G. C. *J. Phys. Chem. B* **2003**, *107*, 668.
(6) Sönnichsen, C.; Franzl, T.; Wilk, T.; von Plessen, G.; Feldmann, O.; Wilson, O.; Mulvaney, P. *Phys. Rev. Lett.* **2002,** *88*, 077402.
(7) Pelton, M.; Liu, M.; Park, S.; Scherer, N. F.; Guyot-Sionnest, P. *Phys. Rev. B* **2006**, *73*, 155419.
(8) Jensen, T. R.; Schatz, G. C.; Van Duyne, R. P. *J. Phys. Chem. B* **1999,** *103*, 2394.
(9) Schoenlein, R. W.; Mittleman, D. M.; Shiang, J. J.; Alivisatos, A. P.; Shank, C. V. *Phys. Rev. Lett.* **1993**, *70*, 1014.
(10) Mittleman, D. M.; Schoenlein, R. W.; Shiang, J. J.; Colvin, V. I.; Alivisatos, A. P.; Shank, C. V. *Phys. Rev. B* **1994,** *49*, 14435.
(11) Park, S.; Pelton, M.; Liu, M.; Guyot-Sionnest, P.; Scherer, N. F. *J. Phys. Chem. C* **2007,** *111*, 116 and references therein.
(12) Hartland, G. V. *Annu. Rev. Phys. Chem*. **2006**, *57*, 403.
(13) Hu, M.; Wang, X.; Hartland, G. V.; Mulvaney, P.; Juste, J. P.; Sader, J. E. *J. Am. Chem. Soc*. **2003,** *125*, 14925.
(14) Del Fatti, N.; Voisin, C.; Chevy, F.; Valee, F.; Flytzanis, C. *J. Chem. Phys.* **1999**, *110*, 11484.
(15) Perner, M.; Gresillon, S.; Marz, J.; von Plessen, G.; Feldmann, J.; Porstenorfer, J.; Berg, K. J.; Berg, G. *Phys. Rev. Lett.* **2000**, *85*, 792.
(16) Okada, N.; Hamanaka, Y.; Nakamura, A.; Pastoriza-Santos, I.; Liz-Marzan, L. *J. Phys. Chem.* **2004**, *108*, 8751.
(17) Hu, M.; Petrova, H.; Wang, X.; Hartland, G. V. *J. Phys. Chem. B* **2005,** *109*, 14426.
(18) Bonacina, L.; Callegari, A.; Bonati, C.; van Mourik, F.; Chergui, M. *Nano Lett.* **2006**, *6*, 7.
(19) Lee, P. C.; Meisel, D. *J. Phys. Chem*. **1982**, *86*, 3391.
(20) Keir, R.; Sadler, D.; Smith, W. E. *Appl. Spect*. **2002**, *56*, 551.
(21) Wilson, O. M.; Hu, X. Y.; Cahill, D. G.; Braun, P. V. *Phys. Rev. B*. **2002**, *66*, 224301.
(22) Kreibig, U.; Vollmer, M. *Optical Properties of Metal Clusters*; Springer: Berlin, 1995.
(23) Kreibig, U. *J. Phys. F: Metal Phys*. **1974**, *4*, 999.
(24) Hövel, H.; Fritz, S.; Hilger, A.; Kreibig, U.; Volmer, M. *Phys. Rev. B* **1993**, *48*, 18178.
(25) Coronado, E. A.; Schatz, G. A. *J. Chem. Phys*. **2003**, *119*, 3926.
(26) Bauer, C.; Abid, J. P.; Fermin D.; Girault, H. H. *J. Chem. Phys*. **2004**, *120*, 9302.
(27) The Fermi velocity oscillates with volume through: $v_F = (h/m)\text{-}(3\pi^2N/V)^{1/3}$.
(28) The effective-scattering length oscillates with volume through $L_{eff} = 4V/S$[25] where S is the surface area.
(29) Benderskii, A. V.; Eloranta, J.; Zadoyan, R.; Apkarian, V. A. *J. Chem. Phys*. **2002**, *117*, 1201.
(30) Eloranta, J.; Apkarian, V. A. *J. Chem. Phys*. **2002**, *117*, 10139.
(31) Pitzer, K. S. *Proc. Natl. Acad. Sci. U.S.A.* **1983**, *80*, 4575.
(32) See, for example, Bard, A. J. and Faulkner, L. R. *Electrochemical Methods*; John Wiley: New York, 2001.
(33) Hartland, G. V. *J. Chem. Phys*. **2002**, *119*, 8048.
(34) Daniels, J. K.; Chumanov, G. *J. Electroanal.Chem.* **2005**, *575*, 203.